

# Magnetic Resonance Imaging of Brain Function and Neurochemistry

KAMIL UGURBIL, DAE-SHIK KIM, TIM DUONG, XIAOPING HU, MEMBER, IEEE,  
SEIJI OGAWA, ROLF GRUETTER, WEI CHEN, SEONG-GI KIM, XIAO-HUNG ZHU,  
ESSA YACOUB, PIERRE-FRANCOIS VAN DE MOORTELE, AMIR SHMUEL, JOSEF PFEUFFER,  
HELLMUT MERKLE, PETER ANDERSEN, AND GREGOR ADRIANY

## Invited Paper

*In the past decade, magnetic resonance imaging (MRI) research has been focused on the acquisition of physiological and biochemical information noninvasively. Probably the most notable accomplishment in this general effort has been the introduction of the MR approaches to map brain function. This capability, often referred to as functional magnetic resonance imaging, or fMRI, is based on the sensitivity of MR signals to secondary metabolic and hemodynamic responses that accompany increased neuronal activity. Despite this indirect link to neurotransmission, recent studies demonstrate that under appropriate conditions, these fMRI maps have accuracy at the scale of submillimeter neuronal organizations such as the orientation columns of the visual cortex, and are directly proportional in magnitude to electrical signals generated by the neurons. High magnetic fields have been critical in achieving such specificity in functional maps because they provide advantages through increased signal-to-noise ratio, diminishing blood-related contributions to mapping signals, and enhanced sensitivity to microvasculature. Equally important is MR spectroscopy studies, which, at high magnetic fields, provide for the first time the opportunity to measure local metabolic correlates of human brain function and neurotransmission rates. Together, these MR methods provide a complementary set of approaches for probing important aspects of the nervous system.*

**Keywords**—BOLD, cerebral blood flow, cerebral oxygenation, cortex, fMRI, functional imaging, magnetic resonance imaging, orientation columns, oxygen consumption, spectroscopy.

Manuscript received December 1, 2000; revised May 23, 2001. This work was supported in part by the NIH under grants P41 RR08079, by a grant from the National Centers for Research Resources (NCRR) division of NIH, by the General Clinical Research Center Program of the NCRR under grants M01RR00400, RO1MH55346, NS38070, NS39043, by the W. M. Keck Foundation, by the Whitaker Foundation, and by the National Foundation for Brain Imaging (NFFBI).

K. Ugurbil, D.-S. Kim, T. Duong, X. Hu, R. Gruetter, W. Chen, S.-G. Kim, X.-H. Zhu, E. Yacoub, P.-F. van de Moortele, A. Shmuel, J. Pfeuffer, H. Merkle, P. Andersen, and G. Adriany are with the Center for Magnetic Resonance Research, University of Minnesota, Department of Radiology, Minneapolis, MN 55455 USA (e-mail: kamil@cmrr.umn.edu).

S. Ogawa is with Bell Laboratories, Lucent Technologies, Murray Hill, NJ 07974-0636 USA.

Publisher Item Identifier S 0018-9219(01)07636-8.

The history of nuclear magnetic resonance (NMR) is marked by an ever increasing number of innovations that have produced novel and surprising uses of this phenomenon for investigating biological processes. No other technique has proven to be so uniquely flexible and dynamic. Since its introduction over 50 years ago [1]–[3], NMR rapidly evolved to become an indispensable tool in chemical and biochemical research because of its sensitivity to the chemical environment of nuclear spins. In 1973, the ability to obtain images with magnetic resonance was introduced [4], leading to the development of magnetic resonance imaging (MRI), which is now solidly established as a research tool and as a noninvasive diagnostic technique in the practice of medicine. At the present time, a major goal in MRI research is the acquisition of physiological and biochemical information noninvasively. The ability to map brain function, often referred to as functional magnetic resonance imaging, or fMRI, is part of this general effort. This development has permitted the examination of functional specialization in the human brain with unprecedented spatial resolution, and has revolutionized cognitive neurosciences.

The most frequently employed fMRI method is based on blood oxygen level dependent (BOLD) contrast, that was first described by Ogawa [5]–[7] in rodent brain studies and subsequently applied to generate functional images in the human brain [8]–[10]. BOLD contrast originates from the intravoxel magnetic field inhomogeneity induced by paramagnetic deoxyhemoglobin (deoxyHb) sequestered in red blood cells, which in turn are compartmentalized within the blood vessels. Magnetic susceptibility differences between the deoxyHb containing compartments versus the surrounding space devoid of this strongly paramagnetic molecule generate magnetic field gradients across and near the boundaries of these compartments. Therefore, signal intensities in MR images sensitized to BOLD contrast are

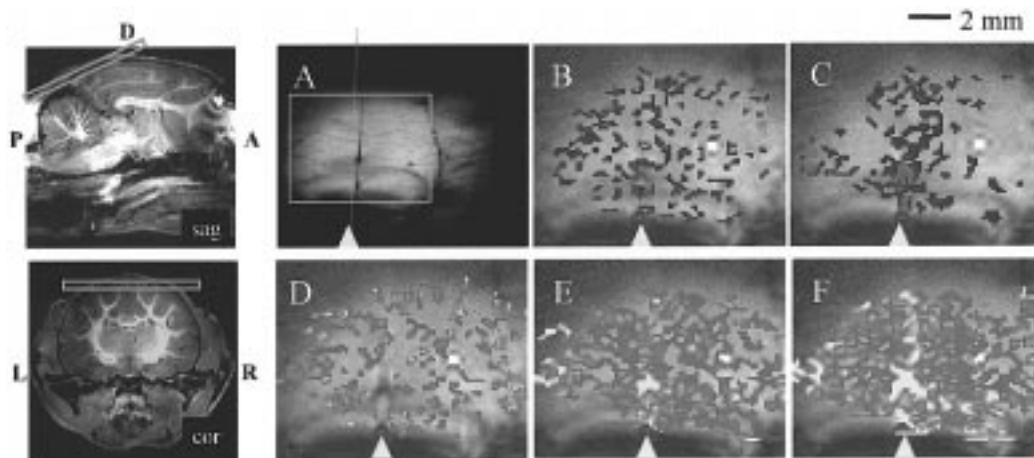


**Fig. 1.** Temporal evolution of the BOLD-based fMRI images in the cat visual cortex. Images are acquired in a plane tangential to the brain and contain the cortical gray matter of the cat visual area 18. The image on the upper left corner demonstrates the orientation of this plane relative to the cat brain and the image obtained from this plane. The pixels that appear patchy and dark relative to the image shown in A represent “activated” regions displaying negative (in B and C) or positive (in D, E, and F) BOLD changes.

altered if the regional deoxyHb content is perturbed. This occurs in the brain because of spatially specific metabolic and hemodynamic responses to enhanced neuronal activity; it has been suggested that regional blood flow (CBF) increases while oxygen consumption rate ( $CMR_{O_2}$ ) in the same area is not elevated commensurably [11]–[13], resulting in decreased extraction fraction and lower deoxyHb content per unit volume of brain tissue. Consequently, signal intensity in BOLD-sensitive images increases in regions of the brain engaged by a “task” relative to a resting, basal state.

In fMRI and other commonly employed functional mapping approaches, such  $^{15}O$  water-based positron emission tomography (PET), functional imaging relies on secondary and tertiary responses to the neuronal activity rather than directly on the neuronal activity itself. Therefore, a crucial question regarding these techniques is how well these secondary and tertiary responses reflect the spatial extent and the magnitude of the neuronal activity. In other words, 1) what is the spatial specificity of the fMRI signals with respect to actual sites of neuronal activity and 2) what is the quantitative link between neuronal electrical activity, neurotransmission, and metabolic and energetic correlates? Recent studies from our laboratory address aspects of these questions and are briefly reviewed in this article.

*Spatial Specificity of fMRI:* Recent studies from our group lead to the conclusion that: 1) spatial specificity of the BOLD response evolves as a function of time after the onset of increased neuronal activity and fMRI signals in steady state or in the late phases of temporal development ultimately lack spatial specificity in the millimeter scale (e.g., scale of iso-orientation domains in the visual cortex) and 2) CBF increases are spatially confined to the activated volume in the iso-orientation domain scale. The first point should, in principle, be anticipated because alterations in deoxyhemoglobin content, whether an increase due to elevated cerebral oxygen consumption rate or decrease due to elevated CBF occur first in the capillary bed. In view of

continuous blood flow, however, these deoxyhemoglobin changes must propagate downstream to blood vessels with ever increasing diameter and ever increasing distance from the actual site of elevated neuronal activity. Ultimately, due to dilution from vessels draining blood from “unactivated” regions, these deoxyhemoglobin changes would come below the sensitivity of detection. However, spatial specificity will be degraded, especially if the activation is confined to a small region of the cortex (e.g.,  $\sim 1$  mm). This is illustrated in Fig. 1 using functional localization in the brain in the submillimeter spatial scale [14], [15].

“Localization” is a principle that is widely used in the brain: parcellation of the cortical tissue into functional subunits is especially prominent at the level of individual cortical columns. Here, neurons with similar response properties, such as ocular dominance and orientation preference in the visual cortex of mammals, are clustered into “columns,” spanning the entire cortical plate from the pia to the white matter [16]–[18]. Since the pioneering work by Hubel and Wiesel [17], the structure, function, and plasticity of cortical columns have been studied using a variety of techniques predominantly based on single and multiunit electrode recordings and optical imaging.

Fig. 1 depicts BOLD MR signals as a function of time in the cat visual cortex during excitation of a single orientation domain [14], [15]. In these studies, the control is a grating that is motionless and the stimulation, which lasts 10 s, is the same grating moving back and forth. Initially, patchy regions associated with elevated deoxyhemoglobin content yielding negative BOLD signals are observed. This patchy image is consistent with what is expected from iso-orientation domains. These early negative signals, however, are not constant in time and migrate toward the sagittal sinus and congregate near and within the sinus. Ultimately, the positive BOLD changes occur and extend over the whole imaged area (visual area 18 of the cat cortex) without any evidence of iso-orientation domains. Clearly, specificity to iso-orien-

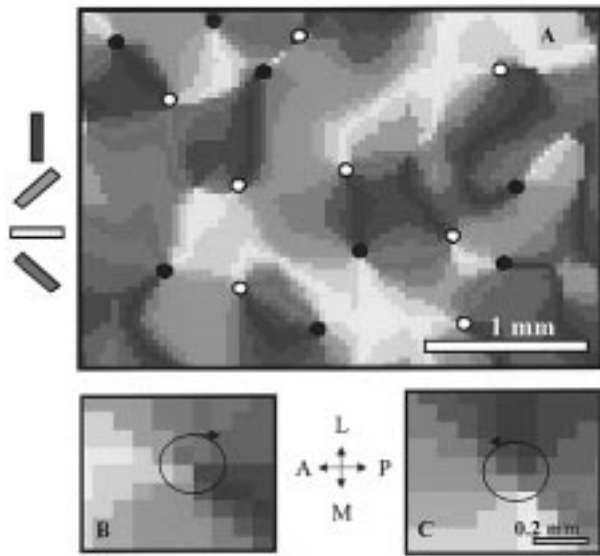


**Fig. 2.** Orientation columns in the cat cortex imaged by early negative bold fMRI. [Scale bar for panel (a): 1 mm. Scale bar for panels (b) and (c): 200  $\mu$ m] Composite-angle map and orientation “pinwheels” generated using “negative” BOLD-fMRI signals during stimulation using moving gratings with different orientations. Panel (a) displays the composite-angle map obtained through pixel-by-pixel vector addition of the four single iso-orientation maps. The resulting orientation preference at each cortical location is gray-scale-coded according to the key displayed to the left of panel (a). Tangent to the cortical surface, the preferred orientations change smoothly, thereby forming a “map” of orientation selectivity. This continuity is interrupted at the “orientation pinwheels” where the cortical columns for different orientations are arranged in a circular manner, thereby forming two types of topological singularities according to their rotational chiralities. The white and black circles in panel (a) depict such “clockwise” and “counterclockwise” pinwheels, respectively. Two such pinwheels are displayed enlarged in panels (b) and (c). The circular arrows in panels (b) and (c) represent the respective directions of change in orientation. A: anterior, P: posterior, M: medial, L: lateral. From [14].

tation domains cannot be present throughout the entire time course of the evolution of the BOLD signals.

When a “composite-angle” map obtained through the vector summation of the four individual iso-orientation maps (corresponding to grating orientations of  $0^\circ$ ,  $45^\circ$ ,  $90^\circ$ ,  $135^\circ$ ) from the initial parts of the early negative response are assembled together and coded in color or gray scale, the well known orientation domains are seen (Fig. 2). In this composite map, the preferred orientations change smoothly, forming a “map” of orientation selectivity, closely resembling those obtained with the optical imaging [19]–[23] and multielectrode recording [24] techniques. The continuity of orientation preferences is interrupted only at the singular points where the domains for all orientations converge. Each orientation is represented only once around such a “pinwheel,” forming two types of topological singularities according to their rotational chiralities. Panels (b) and (c) of Fig. 2 display enlarged pictures of such “clockwise” and “counterclockwise” pinwheels, respectively. In our study, a pinwheel density of  $1.46 \pm 0.17$  pinwheels/ $\text{mm}^2$  ( $n = 4$ ) was found, while optical imaging studies yielded average pinwheel densities between  $1.2 \sim 1.95$  pinwheels/ $\text{mm}^2$

[19], [20], [22]. The ratio between clockwise and counterclockwise pinwheels was found to be roughly 1 : 1 in both fMRI ( $1 : 0.89$ ,  $n = 4$ ) and optical imaging data ( $1 : 0.9$  [22]).

Such orientation maps, however, were not obtained from the maximal positive BOLD response that seem to spread over the entire imaging plane or even the later phases of the initial negative BOLD signal changes (Fig. 1). The results of this study indicate that the temporal evolution of the  $T_2^*$  weighted MR signals from the cat visual cortex is biphasic as noted in earlier high field MR studies of the human visual cortex [25]–[29] and optical imaging experiments on the cat cortex [30], [31]. Furthermore, they demonstrate that the initial decrease of BOLD signals accurately yield individual iso-orientation columns, while the later phases of the negative response and the subsequent positive BOLD changes were largely incapable of differentiating between active and inactive columns [14], [15].

The early transient increase in deoxyhemoglobin content corresponding to the early negative BOLD changes are thought to arise from an increase in  $\text{CMRO}_2$  that precedes the elevation in CBF. The CBF increase ultimately overcomes the increased deoxyhemoglobin generated by the elevated  $\text{CMRO}_2$  and leads to a hyperoxygenated state.  $\text{CMRO}_2$  alteration must occur locally coincident with the volume of elevated neuronal activity. Their detection through deoxyhemoglobin changes, therefore, is expected in the early time points, before deoxyhemoglobin alteration propagates downstream in the vasculature. Early blood volume changes, and processes such as penetration of red blood cells into capillaries that were previously devoid of them can also explain the early negative BOLD effect. However, early  $\text{CMRO}_2$  changes that correlate in time with the early negative BOLD response do exist [32] and must be at least part of the explanation of the fMRI data.

The lack of spatial specificity in the later parts of the BOLD response, especially in the positive BOLD effect can have two possible explanations. First, as already mentioned, the deoxyhemoglobin decrease or increase that occurs initially in the activated area propagates “downstream” in the vasculature due to blood flow and will consequently be detected in draining large veins distant from the region of interest. There is also a second possible explanation, which is that the CBF response to alterations in neuronal activity is not controlled at the iso-orientation column level and, therefore, does not have spatial specificity in this spatial scale. The initial decrease in the BOLD signal reflecting increased deoxyhemoglobin is reversed because of CBF increase coupled to elevated neuronal activity. The fractional increase in CBF is larger than the fractional increase in oxygen consumption rate, resulting in a significant drop in deoxyhemoglobin content and a positive BOLD signal. The spatial extent of this positive BOLD signal will reflect, therefore, the spatial extent of the CBF response.

The lack of spatial specificity in the CBF response in the orientation-column scale has previously been suggested based on optical imaging data [31]. However, optical methods do not measure CBF directly; rather, CBV is experimentally determined and usually taken to correspond

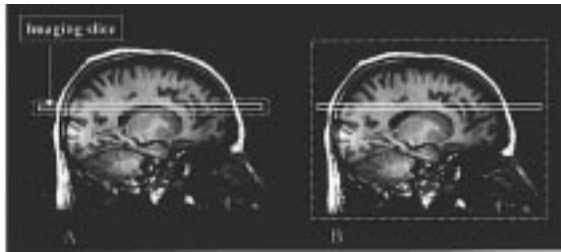


**Fig. 3.** The FAIR technique subtracts two images where the only difference is the spatial selectivity of the inversion pulse that always precedes the image acquisition. In one image (A), the inversion pulse is slice selective and ideally should have the same dimensions as the imaging slice; because of pulse imperfections at the edges, the inversion slice is typically a little larger. In the second image (B), the inversion pulse is nonselective but, nevertheless, it has a spatial extend due to the RF coil used which covers only the brain and part of the neck.

to CBF. Recent magnetic resonance imaging techniques, however, can generate images based on quantitative measures of CBF changes coupled to neuronal activity [8], [33]–[37]. These CBF techniques rely on tagging the blood spins differentially within and outside of a well-defined volume. For example, in the FAIR technique [33], [35], [36], frequency-selective inversion pulses are used to invert the longitudinal magnetization within a “slab” along one direction (typically axial) (Fig. 3); in the absence of blood flow, the spins relax back to thermal equilibrium only by spin-lattice relaxation mechanisms characterized with the time constant  $T_1$ . If flow is present, however, the relaxation becomes effectively faster as unperturbed spins outside the inverted slab flow in and replenish the net magnetization within the slab. Consequently, the effective spin-lattice relaxation in FAIR as well as other similar flow-sensitive techniques [33], [38]–[42] becomes characterized by a shorter time constant,  $T_{1^*}$ , which is related to blood flow. It also follows naturally that if the inversion pulse in FAIR does not define a slab but inverts everything in the whole body (i.e., it is nonselective), blood flow does not enter into to the problem at all. Thus, in the FAIR technique, two images are acquired consecutively, each after a fixed delay period subsequent to the inversion pulse; in one, the inversion pulse is slab selective and in the other it is nonselective. The difference image generated from this pair is a flow sensitive image. Fig. 4 illustrates the results of such a “blood flow” based functional imaging study in the human brain at 4 T, acquired during a finger movement task. The gray scale image depicts CBF which is high in the gray matter areas that contain the cell bodies and the dendrites, and low in the white matter that is primarily composed of axons connecting the neurons. As expected, these CBF images resemble anatomical images that distinguish gray and white matter in the brain. However, in case of the blood flow image, the signal intensity can be quantitated and assigned a number in terms of milliliters of blood delivered per minute to a gram of brain tissue [33], [35].

One of the unique aspects of CBF-based functional maps is that macrovascular flow components can be selectively suppressed while sensitivity to microvascular flow and tissue

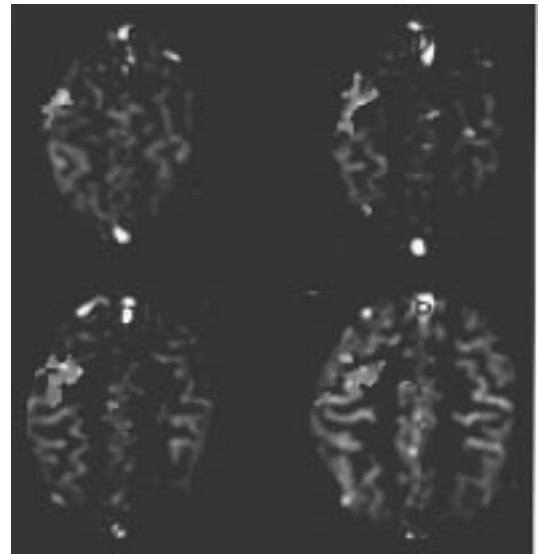


**Fig. 4.** Multislice study of finger opposition task examined with FAIR technique, measuring blood flow changes [35]. The gray scale image depicts signal intensity proportional to blood flow. Superimposed map identifies regions of the brain where blood flow changed during the tasking period. Note the excellent correspondence of the functional map with gray matter areas identified by the higher intensity regions in the gray scale map. Gray matter has higher blood volume and blood flow than white matter. Consequently, the FAIR images have higher intensity in the gray matter areas.

perfusion changes is enhanced. In an experiment like FAIR, this selective microvascular sensitivity is accomplished by changing the delay time after the initial inversion pulse and the subsequent signal excitation before image acquisition. In CBF-based functional imaging, longer delays ( $>1$  s) emphasize microvascular flow and perfusion whereas shorter delays yield predominantly large vessel images [33], [43]. The former, of course, is highly desirable for generating functional maps. The accuracy of CBF-based functional maps was recently demonstrated using rat forepaw stimulation and  $Mn^{++}$  contrast.  $Mn^{++}$  is an analog of the  $Ca^{++}$  ion that is involved in neurotransmission.  $Mn^{++}$  can enter into neurons during  $Ca^{++}$  uptake. In animal models, transiently breaking the blood brain barrier permits the infusion of  $Mn^{++}$  into the brain and leads to increased uptake and accumulation of this ion in neurons that are activated and are engaged in elevated neurotransmission [44], [45]. The presence of  $Mn^{++}$  can be detected by MRI because  $Mn^{++}$  is a strongly paramagnetic molecule and shortens the  $T_1$  relaxation rate of the tissue water. Thus, functional images based on  $Mn^{++}$  accumulation can be detected in  $T_1$  weighted images. When this approach was used during rat forepaw stimulation and the results compared with CBF-based functional maps, excellent correspondence was demonstrated and both displayed images that were specific to layer 4 of the cortical gray matter, as expected. This is illustrated in Fig. 5.

The hypothesis that CBF is not spatially specific was examined recently in our laboratory using CBF-based functional mapping of orientation columns in the cat cortex using. These experiments demonstrated that CBF (i.e., perfusion) response also give highly accurate orientation maps in the

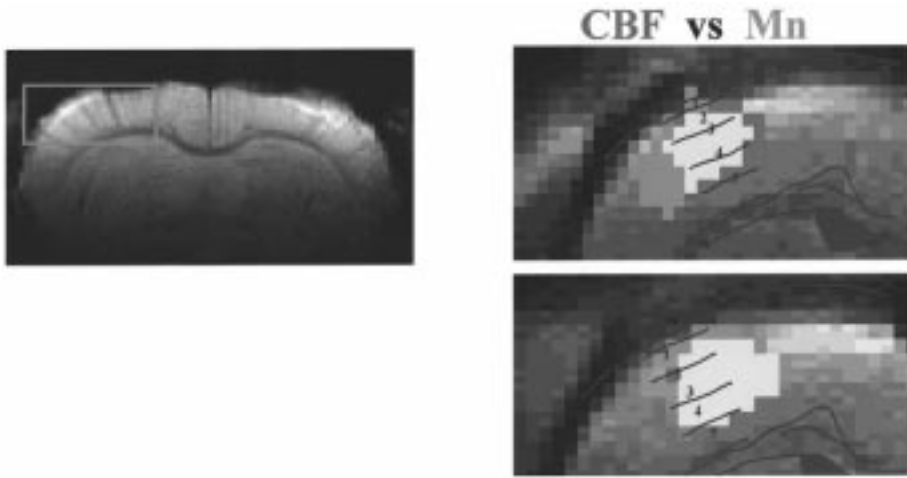


**Fig. 5.** Comparison of CBF and  $Mn^{++}$ -based functional maps in the rat cortex. The dashed lines indicate the layers in the rat cortex. From [79].

visual cortex of the cat and are spatially specific at this scale [46]. Thus, the lack of specificity in the positive BOLD response does not reflect a lack of specificity of the underlying CBF; instead, it is likely to be due to the blood flow induced propagation of the deoxyhemoglobin alterations into the large blood vessels which, naturally, do not correspond accurately to the actual site of activation in millimeter to sub-millimeter scale.

*Approaches to Spatially Specific Mapping Using the Positive BOLD Response:* While CBF appears to be highly spatially specific and provides a means by which accurate fMRI can be performed, it is still not the preferred approach in generating functional maps. The reason is that contrast-to-noise (CNR) is higher in BOLD images and in particular, rapid acquisition covering the whole or a large subsection of the brain remains to be developed with CBF-based methods. In particular, the method is more challenging in human applications because of signal-to-noise limitations and long transit times for blood. Unlike the CBF-based techniques, however, BOLD images can be acquired rapidly over the whole brain. The early negative BOLD response also suffers from signal-to-noise limitations because it is such a small effect. Thus, the positive BOLD effect approach remains the main method employed in fMRI applications. The question arises then as to how one can acquire fMRI images based on the positive BOLD effect but has the spatial specificity in the columnar domain. One promising approach is to use  $T_2$  rather than  $T_2^*$  weighted BOLD images at very high magnetic fields. The rationale for this is explained below.

In the blood, hemoglobin is compartmentalized within red blood cells. Thus, when the deoxy form is present, there are magnetic field gradients around the red cells. However, because the dimensions are very small compared to diffusion distances, the effect is dynamically averaged by diffusive motion of the water molecules (Fig. 6) and becomes a  $T_2$  effect only, as opposed to a  $T_2^*$  effect. The dynamic averaging in this case also involves exchange across the red blood cell membrane that is highly permeable to water. Thus, in the presence

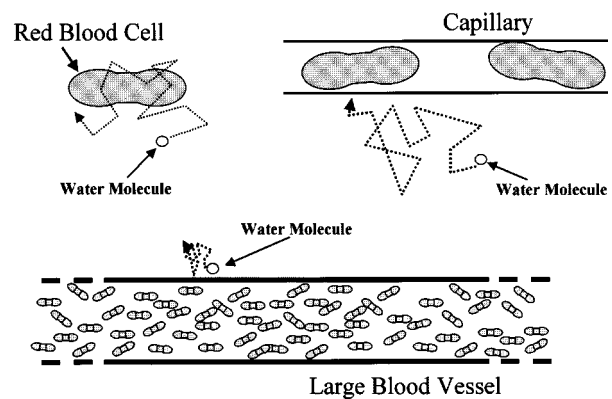


**Fig. 6.** Dynamic and static averaging regimes based on diffusion distances relative to the size of the compartment that differs in magnetic susceptibility compared to the surrounding tissue. The magnetic field gradients are most prominent in the vicinity of the compartments with different susceptibility, i.e., red blood cells, capillaries, and large blood vessels. In case of the large blood vessels, diffusion distances are not large compared to vessel radius, and, hence, do not lead to dynamic averaging.

of deoxyhemoglobin containing red blood cells,  $T_2$  of blood decreases. This effect was noted by Thulborn [47], [48] and was shown to increase quadratically with field strength as expected. Therefore, the  $T_2$  of *blood itself* will change when the deoxyhemoglobin content is altered by elevated neuronal activity and this will lead to a signal change in a BOLD weighted image. This *intravascular* BOLD effect will be present wherever the deoxyhemoglobin content alteration occurs, thus potentially both in large and small blood vessels.

The *extravascular* BOLD effect is associated with the magnetic field gradients generated outside the luminal boundaries of the blood vessels due to the deoxyhemoglobin induced magnetic susceptibility difference between the blood vessel and the surrounding diamagnetic tissue. When these blood vessels are small (for  $4\text{ T} \sim 5\ \mu\text{m}$  given the typical deoxygenation state of the capillary/venous blood), these magnetic field gradients are dynamically averaged and result in a  $T_2$  effect just like the intravascular BOLD

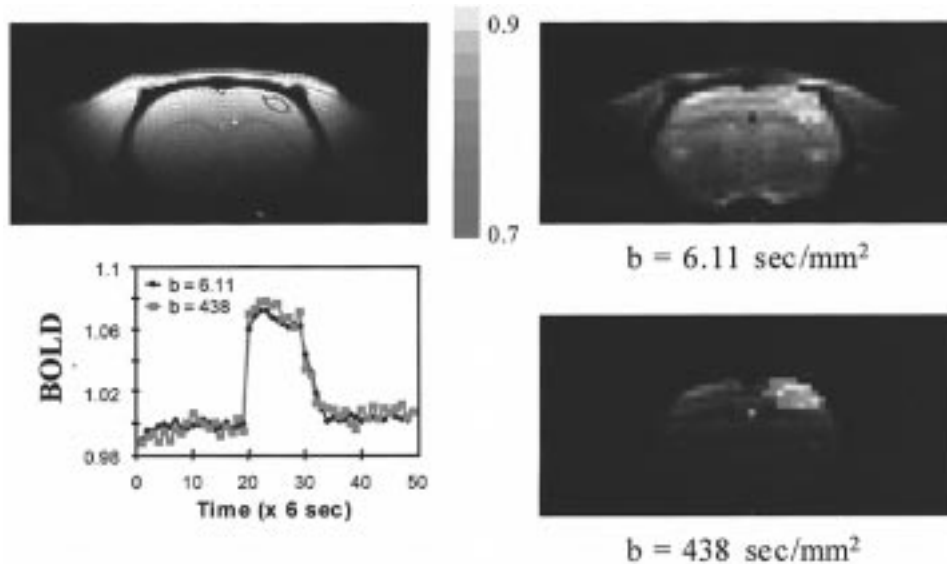


**Fig. 7.** 9.4 T Diffusion-weighted spin-echo fMRI maps with  $b$  values of 6.1 (top right) and 438  $\text{s/mm}^2$  (bottom right) overlaid on one of the original, consecutively acquired EPI images (BOLD and diffusion weighted) collected during the functional imaging study. Coronal single-slice single-shot spin-echo EPI images of rat brain were acquired with a matrix size of  $64 \times 32$ , a FOV of  $3.0 \times 1.5 \text{ cm}^2$ , a slice thickness of 2 mm, and  $\text{TE} = 30 \text{ ms}$ . Somatosensory stimulation was used. Bar indicates a maximum cross-correlation value from 0.7 to 0.9. Signal intensity (shown in background) was significantly reduced by bipolar gradients, as expected due to diffusion. Localized activation is observed at the somatosensory cortex in the contralateral side of a stimulated forepaw. Foci of activation site agree very well in both fMRI maps. A Turbo FLASH image with a region of interest is shown in the upper left corner and time courses of diffusion-weighted images within the ROI are shown in the bottom left corner. If the macrovascular contribution were significant, relative BOLD signal changes would decrease when a higher  $b$  value is used. However, relative signal changes remained the same in both images, suggesting that extravascular and microvascular components predominantly contribute to spin echo BOLD at 9.4 T. From [54].

effect. However, when the blood vessel dimensions are large, dynamic averaging is not possible. Instead, there will be “local” or “partial” dynamic averaging over a subsection of the volume spanned by the magnetic field gradients generated by the blood vessel (Fig. 6). However, there will be signal loss from the voxel due to *static averaging* if refocusing pulses are not used. A water molecule at a given point in space relative to the blood vessel will see a “locally” time-averaged precession frequency,  $\bar{\omega}_B$ , which will vary with proximity to the large blood vessel. Because  $\bar{\omega}_B$  varies across the voxel, signal for the entire voxel will be “dephased” and lost during the delay employed in BOLD weighting after signal excitation and prior to signal acquisition (echo time TE). This signal loss occurs from “*static averaging*.” In this regime, if the variation  $\bar{\omega}_B$  over the voxel is relatively large, signal decay can be approximated with a single exponential time constant  $T_{2^*}$ . In a spin-echo experiment, this static averaging is eliminated and will not come into play since the dephasing will be reversed after the application of a  $180^\circ$  pulse prior to signal acquisition.

The origin of the signal intensity changes that are detected in  $T_2$  versus  $T_{2^*}$ -based BOLD fMRI images differ significantly.  $T_{2^*}$ -based BOLD signal can arise from both intravascular (blood) and extravascular effects originating from large and small blood vessels. The relative contributions of these effects depend on the magnetic field strength. In a  $T_2$ -based BOLD fMRI map, the signal changes come from: 1) intravascular, blood  $T_2$  changes, hence both from large and small

blood vessels and 2) extravascular effect associated *only with microvessels* such as capillaries and small venules. Thus, the major difference is that the *extravascular* BOLD effect in a  $T_2$  image can only arise from the microvasculature. Therefore, if the blood-related intravascular effects can be suppressed, a  $T_2$ -based BOLD response will be sensitive to *only* microvasculature.

The issue of extra- versus intravascular BOLD effect has been experimentally examined using bipolar gradients. In an fMRI experiment, images are collected subsequent to signal excitation and echo formation, either by a gradient reversal or application of a refocusing RF pulse. During the delay after excitation and before echo formation, it is possible to apply a pair of gradient pulses with opposing or same polarity depending on whether the experiment is a gradient recalled- or a spin-echo experiment, respectively. When the water molecules are static in time, then such gradient pulses will ideally have no effect on the image. In the presence of diffusion, such pulses will lead to signal loss since the spatially dependent dephasing during first part of the gradient pulses will not be redone during the second gradient pulse. This pulsed gradient pair has been introduced for diffusion measurements by Stejskal and Tanner [49]; hence, often the use of such gradients to alter the image signal intensity is referred to as “diffusion weighting” even though there are additional perturbations that arise from the use of such gradients.

In experiments employing the Stejskal–Tanner gradients, the important parameters are the magnitude and the duration

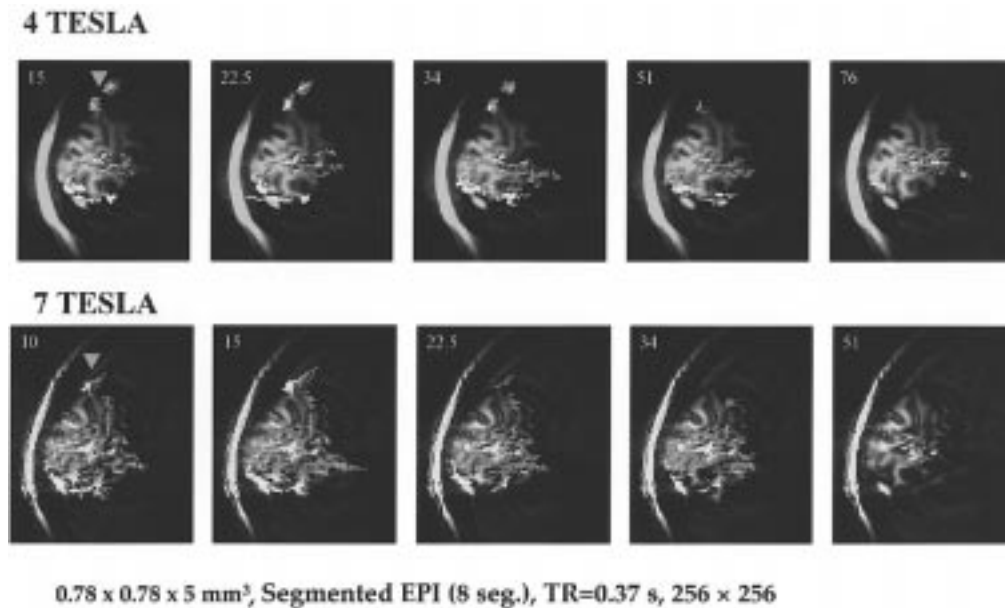


**Fig. 8.** (a) Activation maps obtained at different TEs in one subject at 4 T (top) and 7 T (bottom). TEs in milliseconds are marked in the maps. (b) Time courses for TE of 22 ms at 7 T and TE of 30 ms at 4 T.

of the gradient pulse and the time separation between them. Frequently, the results are evaluated in terms of a parameter  $b$  which is equal to  $(\gamma G \delta)^2 (\Delta - \delta/3)$  where  $\gamma$  is the gyromagnetic ratio (rad/s/Gauss),  $G$  is the magnetic field gradient magnitude (Gauss/cm),  $\delta$  is the duration of the gradient pulse, and  $\Delta$  is the separation in time of the onset of the two gradient pulses. In simple isotropic diffusion, the MR signal in the presence of Stejskal–Tanner gradients decays according to  $\exp(-bD)$  where  $D$  is the diffusion constant. For flowing spins,  $b$  does not have such an immediately obvious physical meaning. If there is flow, the spins will acquire a phase that depends on amplitude of the Stejskal–Tanner gradients, the position of the spin, and the velocity of the spins. Within blood vessels, however, flow is not uniform especially for large diameter vessels. Furthermore, the blood vessels may change directions within a voxel, and there may be several different blood vessels within the voxel with different flow rates and/or different orientations relative to the gradient directions. Since the blood signal detected from the voxel will be a sum of all of these, the net result can be signal cancellation due to dephasing of flowing spins. As a result, these pair of gradients can effectively suppress flowing spins in blood vessels.

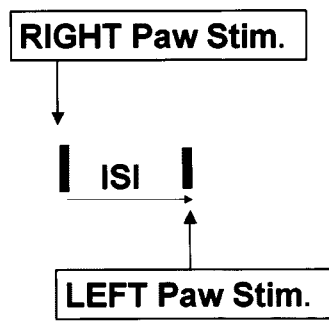
The Stejskal–Tanner pulsed gradients can be used to distinguish between intra- and extravascular BOLD effects in functional images. Such experiments have been performed at 1.5 and 4 T on humans. The studies at 1.5 T have concluded that most of the BOLD-based signal increase during elevated neuronal activity is eliminated by bipolar gradients, leading to the conclusion that most of the fMRI signal at 1.5 T arises from *intravascular* effects [50], [51]. One can even suggest that this intravascular BOLD effect may be associated with only macroscopic blood vessels since it is debatable as to whether the gradient pulses used can suppress intravascular signals from microscopic blood vessels such as cap-

illaries and small venules [52]. When similar studies were performed with 4 T, ~60% of the “activated” pixels disappeared at small  $b$  values but the remaining pixels persisted as the gradient strength was increased to attain very large  $b$  values. This suggested that, at 4 T, there exist *extravascular* and/or *capillary-level intravascular* BOLD effect during activation in addition to a significant intravascular contribution associated with macrovasculature.

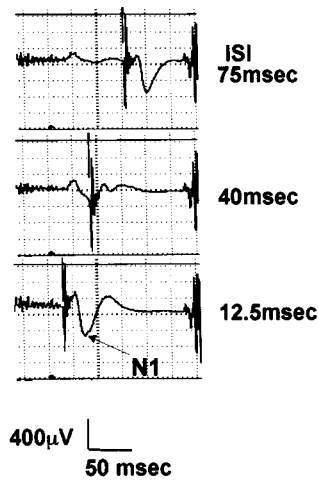
At 9.4 T, the effect of the Stejskal–Tanner gradients becomes more interesting. In a  $T_2$  weighted fMRI study conducted in the rat brain (forepaw stimulation, symmetric spin-echo with one  $180^\circ$  pulse), we observed that the activation is not altered at all going from very small to very high  $b$  values (Fig. 7).  $T_2$ -based BOLD effect can only come either from blood due to a change in the blood  $T_2$  or from extravascular effects associated with capillaries and comparably sized venules. The gradient pair will suppress the blood, except possibly in capillaries and small venules. Therefore, one can conclude that at this ultrahigh magnetic field, there exists a strong and dominant BOLD effect originating from microscopic vessels only. However, as previously discussed, blood itself can yield  $T_2$ -based changes in fMRI signals. This is not detected at 9.4 T. The reason for this turns out to be the very short  $T_2$  of venous blood itself at the very high magnetic field ( $\sim 5$  ms at 9.4 T). Even arterial blood has a short  $T_2$  at this high magnetic field strength ( $\sim 30$  ms).

With the installation of a 7 T whole body system in our laboratory, we have recently begun similar experimental fMRI studies in humans for the first time at magnetic field strengths that significantly exceed 4 T. The experiments were conducted using a surface coil with a visual stimulation paradigm. While investigation of the  $T_2$  BOLD effect is presently ongoing at 7 T in the human brain and, as such, it is not suitable for this review, experiments have already been conducted with  $T_2^*$

## PARADIGM

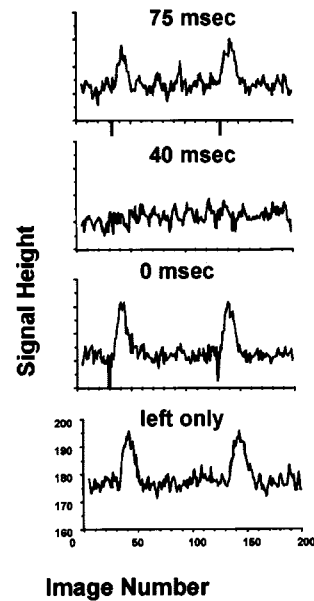


## SEP (somatosensory evoked Potential)



(a)

## fMRI



(b)

**Fig. 9.** Stimulation at two forepaws with time delay (a) SEP responses at the contralateral somatosensory area to the left forepaw. Top: ISI 75 ms. Middle: 40 ms. Bottom: 12.5 ms. The noises after the evoked potentials were EPI generated. The sharp spikes at the second stimulation were electrical artifacts. (b) The time courses of BOLD responses (without EEG electrodes) with varied ISI. (From [59].)

BOLD that are relative and are indicative of increased spatial specificity. These studies are briefly summarized here.

Fig. 8 displays activation maps obtained from one subject at several TEs for both 7 T and 4 T. At the same statistical threshold, the 7 T maps exhibited considerably larger activated area at all TEs except the last one. A paired t-test for the number of activated pixels (averaged over all TEs) between the 7 T and 4 T data showed that the 7 T maps were significantly ( $p < 0.008$ ) larger than that of the 4 T data. As expected, the activation maps in Fig. 8 varied with TE and became most prominent at a certain TE, depending on the field strength. In the gray matter, signal change ( $\Delta S$ ) induced by the positive BOLD effect had a maximum at a TE of 25 ms at 7 T, and 35 ms at 4 T, consistent with the theoretical prediction that there is a maximum for activation induced signal change which occurs when  $TE = T_2^*$ . Consistent with the rapid decrease in venous blood  $T_2$  and  $T_2^*$  with increasing magnetic field [53], [54], the large venous vessel (sagittal sinus) contributions to functional maps (see arrow in Fig. 8) disappeared in the 7 T activation maps at long TEs while the same vascular contribution remained prominent with increasing TE at 4 T. A separate measurement of *ex vivo* human venous blood found the  $T_2$  to be approximately 7 ms for blood with normal  $O_2$  saturation (subject 1:  $T_2 = 6.8 \pm 0.4$  ms,  $Y = 38\%$ ; subject 2:  $T_2 = 7.1 \pm 0.7$  ms,  $Y = 39\%$ ; subject 3:  $T_2 = 13.1 \pm 0.2$  ms,  $Y = 59\%$ ). These awake human fractional oxygenation levels are significantly lower in the relative to the anesthetized animals ( $Y \sim 80\%$  in the animal model in the 9.4 T study [54]). Because of this difference, the susceptibility gradient surrounding red blood cells

at 7 T in humans will be comparable or larger than those in the 9.4 T animal model study. Therefore, the suppression of blood contribution to functional images due to the increased field will be comparable in the two studies.

The 7 T human studies demonstrate that all blood-related mechanisms that contribute to the BOLD effect (see discussion in [55]–[57]) are virtually inoperative at 7 T for TEs equal to or exceeding the optimum TE of 25 ms while they are still significant at the optimum TE of 35 ms at 4 T. This has important implications with respect to the specificity of the human functional images at 7 T since such blood-related effects are mostly associated with large blood vessels and, as previously mentioned, dominate 1.5 T [50], [51], [58] and even 4 T [55]–[57] brain activation maps.

In the absence of the above-described BOLD mechanism related to blood effects, macroscopic venous blood vessels can only contribute to  $T_2^*$ -weighted images at 7 T through the extravascular BOLD mechanism arising from static averaging of field gradients around these vessels. Such effects, however, are eliminated in  $T_2$ -based BOLD studies. Therefore, provided the  $T_2$ -based BOLD response is large enough, this approach should become a useful method for obtaining highly specific functional images.

The problem faced with  $T_2$ -based imaging is not just the elimination of the blood contribution, however, which occurs naturally at high magnetic fields. After all, as demonstrated effectively, “diffusion” weighting gradients can suppress the blood-related effects associated with large veins. So, why not use  $T_2$ -weighted BOLD fMRI with “diffusion” weighting at 1.5 T for obtaining accurate functional maps? The reason is

that once the blood-related effects are significantly reduced, the remaining  $T_2$  BOLD effect associated with microvasculature are intrinsically very small at 1.5 T due to the time averaging process itself. Therefore, at lower magnetic fields this approach suffers from contrast-to-noise ratio limitations when the blood effects originating from large blood vessels are eliminated. However, the effect increases rapidly with magnetic field. We see that at 9.4 T, it yields 10% signal changes associated with activation (Fig. 7).

**Quantitative Link Between fMRI Signals and Neuronal Activity:** In electrophysiological studies of brain, such as single unit recording of spikes, increased spike rate directly and quantitatively reflects increased rate of firing of a neuron or a group of neurons. Such quantitative measurements are critical in understanding brain function. It has generally been assumed that a link does not exist in fMRI because of the rather complicated nature of the fMRI response and its indirect link to increased neuronal activity. Surprisingly, however, recent experiments demonstrate that at least for relatively short stimulation periods, the two are linearly dependent. An example of this from our recent paper [59] is illustrated in Figs. 9 and 10 using an experiment where two  $\sim 300$ -ms-long electrical stimulations, separated by a variable interstimulus interval (ISI) is applied; the first one to the left paw and the second one to the right paw of a rat. Both somatosensory evoked potentials (SEM), and BOLD-based fMRI from the region corresponding to the right paw are monitored. We see that when ISI is  $\sim 40$  ms, SEM virtually disappears, presumably due to an inhibitory effect originating from regions activated by left paw stimulation and traveling in  $\sim 40$  ms to the site of activity induced by the right paw stimulation. For ISIs that are much shorter or longer than  $\sim 40$  ms, the inhibition in the SEM is not observed. The same is detected in the BOLD fMRI signals (Fig. 9). The normalized BOLD and SEM data when plotted as a function of time display a decrease around  $\sim 40$  ms (Fig. 10). When these data are rearranged as normalized BOLD versus SEM, we see a linear relationship (Fig. 10).

It should be noted that these data also demonstrate that using this approach, the amplitude modulation in BOLD can be used to monitor temporal evolution of neuronal activity in the neuronal time scale. This time scale is in tens of milliseconds and is not normally accessible to fMRI approaches due to the slow CBF and  $CMRO_2$  responses to increased neuronal activity.

**Neurochemistry by MR Spectroscopy:** In addition to MR imaging that utilizes protons of tissue water, magnetic resonance plays an increasingly important role in detecting neurochemicals directly and noninvasively in the brain, including the human brain. This capability is based on the sensitivity of the resonance frequency of nuclear spins to their chemical environments (i.e., the chemical shift effect). This type of MR data, referred to as magnetic resonance spectroscopy (MRS), can be performed with spatial localization so that signals can be obtained from a well-defined region in the space.

Spatially localized MRS has been employed to measure aspects of brain function and neurotransmission directly.

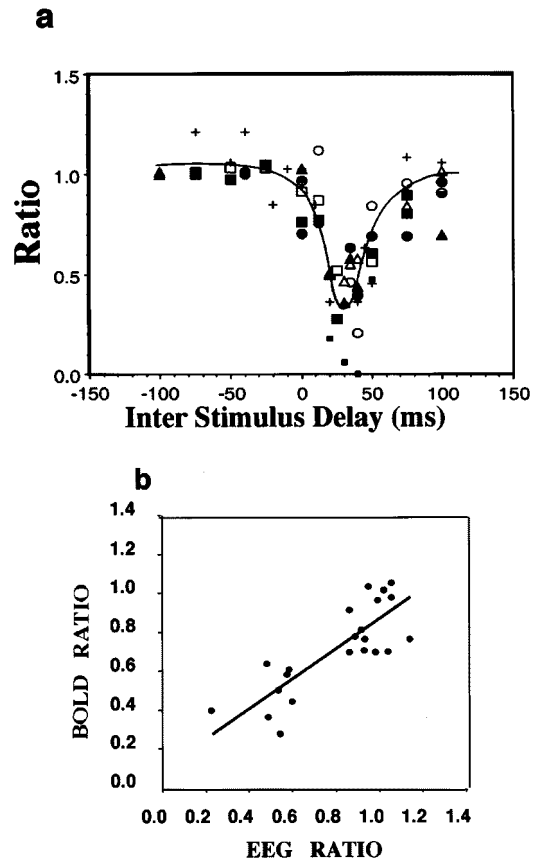


**Fig. 10.** The time window of suppression of somatosensory evoked potential (SEP) and BOLD responses with the two-forepaw stimulation paradigm as in Fig. 9. The symbols ( $\Delta$ ) are those of SEP measurements only and filled circle symbols are those of MRI measurements without EEG electrodes. Open square symbols are SEP and filled square symbols are BOLD responses in simultaneous measurements. All responses were normalized to the respective values at ISI of  $-100$  ms (left stimulation first), or the values with left stimulation only. The curve was drawn to represent the SEP responses [59].

Recent efforts have focused on understanding the coupling between cellular bioenergetics and neuronal activity (e.g., [60]–[67]). The  $^{13}\text{C}$  nucleus, the only NMR-detectable, stable carbon isotope that is normally present at 1.1% abundance, has played an important role in these efforts. If  $^{13}\text{C}$ -enriched glucose is given to a living organism, the  $^{13}\text{C}$  label is incorporated through metabolism into several positions in many different compounds. Of interest is the incorporation of the label into the intermediates of tricarboxylic acid (TCA) cycle, which generates reducing equivalents utilized in oxygen consumption. The label is then transferred into the amino acids glutamate, aspartate, and glutamine. The ability to monitor the labeling of intracellular compounds in intact cells was first demonstrated using *E. coli* [68]. Today, using advanced shimming techniques [69] and three-dimensional localization methods, such highly specific data can be obtained in human and animal brains from relatively small-volume elements (e.g., [63], [65], [70]–[72]).

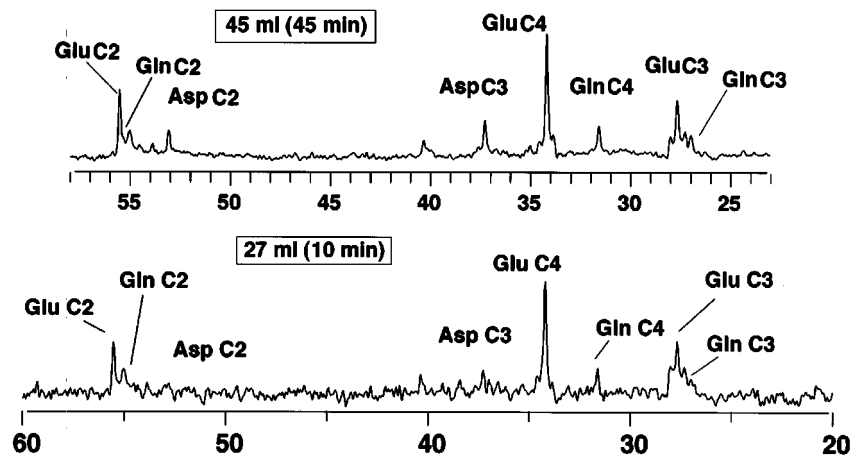


**Fig. 11.**  $^{13}\text{C}$  NMR spectrum acquired from a volume localized in the human visual cortex obtained at 4 T. Glutamatergic neurotransmission rate and oxygen consumption rate can be calculated from a spectra obtained as a function of time. Signals from multiple carbons of various amino acids and neurotransmitters are detected. Asp: aspartate. Gln: glutamine. Glu: glutamate. GABA, NAA: N-acetyl aspartate. (From [65].)

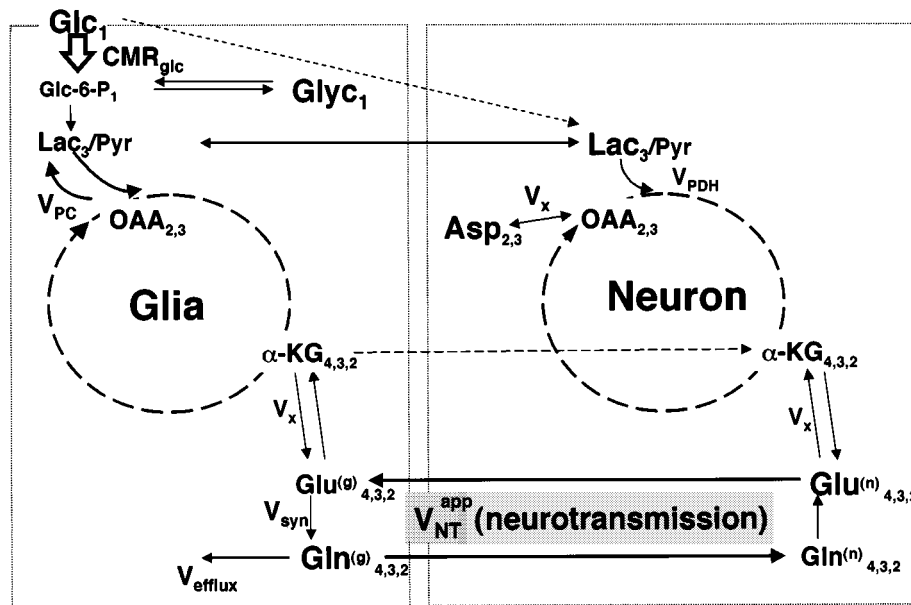


**Fig. 12.** Metabolic pathways in neurons and glia that can be modeled by  $^{13}\text{C}$  NMR data. (From [65].)

The human brain  $^{13}\text{C}$  spectra in Fig. 11 (obtained at 4 T in our laboratory) illustrate the detection of many labeled compounds from a *relatively small, localized region* in the visual cortex, and the first time measurement of neurotransmission rate in the *human* visual cortex [65]. A subsequent effort on humans at 2.1 T [66] was able to report basically the same results, but used at least threefold larger volumes (144 ml versus 45 ml) and longer data acquisition times for signal detection due to the lower field employed. In these studies, it is possible to extract information from the compartmentalized metabolic pathways illustrated in Fig. 12. Most important is the glutamate–glutamine cycling between glia and the neurons, the two major cell types that are present in the brain: Glutamate is the major excitatory neurotransmitter. Once it is released into the synaptic cleft and binds the post-synaptic

receptors during neurotransmission; it is scavenged rapidly by nearby glial processes [73], [74]. Glutamate is then converted to glutamine by glutamine–synthase, which is present only in the glia [75]; glutamine is subsequently transported to the neurons, converted to glutamate to replenish vesicular glutamate. Thus, glutamine labeling in  $^{13}\text{C}$  experiments can in principle occur predominantly through glutamate release through neurotransmission and, hence, reflect the kinetics of neurotransmission. Therefore, from such  $^{13}\text{C}$  studies, it is possible to calculate rates of glutamatergic neurotransmission ( $V_{\text{NT}}$ ), TCA cycle turnover, cerebral oxidative glucose utilization ( $\text{CMR}_{\text{glu}}$ ) and even break down the latter into glial and neuronal contributions (Table 1). The most important finding from our studies is the conclusion that  $V_{\text{NT}}$  equals  $\sim 60\%$  of total oxidative glucose consumption rate in the

**Table 1**

Metabolic Fluxes ( $\mu\text{mol g}^{-1} \text{min}^{-1}$ ) and Ratios Derived From the Human Visual Cortex the Model Shown in Fig. 12

$\text{CMR}_{\text{glc}} (\text{ox.})$	$= 0.41 \pm 0.03$	(Oxidative glucose consumption)
$V_{\text{NT}}$	$= 0.26 \pm 0.10$	(neuro-transmission)
$V_{\text{PDH}}$	$= 0.57 \pm 0.06$	(Pyruvate Dehydrogenase)
$V_{\text{PC}}$	$= 0.09 \pm 0.02$	(Pyruvate carboxylase)
$V_x$	$= 0.57 \pm 0.19$	( $\alpha$ Ketoglutarate - Glutamine exchange)

Neurotransmission/Oxidative glucose consumption Rates =  $0.41 \pm 14$

Glial/ Neuronal ATP synthesis  $\sim 17\%$

Oxidative vs. Total ATP synthesis in Glia  $< 60\%$

brain and that there is significant oxidative ATP production rate in the glia, apparently in contradiction with earlier conclusions reached from experiments on the anesthetized rat brain data [76].

Such detailed studies have not yet been applied to investigate neuronal activation in the human or animal brains due to limitations in signal-to-noise ratio of the measurements. However, a subset of the data in the direct  $^{13}\text{C}$  measurements can be acquired with indirect detection with higher sensitivity using the protons attached to the  $^{13}\text{C}$  nuclei, permitting calculations of changes in TCA cycle turnover and oxidative  $\text{CMR}_{\text{glu}}$  during neuronal activation. The experiment demonstrating this is illustrated in Fig. 13, where hemifield visual stimulation was used to obtain spectroscopic data (together with CBF and BOLD fMRI) from an activated region in one hemisphere while the other hemisphere served as control [61], [77].

The study illustrated in Fig. 13 is concerned with the coupling of oxidative metabolism and neuronal activity. It is well known that under resting conditions, the cerebral metabolic rate of glucose consumption ( $\text{CMR}_{\text{glc}}$ ) is well coupled to  $\text{CMR}_{\text{O}_2}$  as well as to cerebral blood flow (CBF) in the human brain [78] and references therein), and the glucose metabolism is almost completely through oxidation. However, this appears not to be the case during increased neuronal activity. Based on PET studies, the increases of  $\text{CMR}_{\text{O}_2}$  (0%–5%) were found to be much less than the elevation in CBF and  $\text{CMR}_{\text{glc}}$  (40%–51%) during visual and somatosensory stimulations [11], [12]. This early PET result remains to this day highly debated, with the intensity of debate having increased recently in view of its significance in understanding the BOLD response that has come to play such a prominent role in neuroscience research. The difficulties and complexities associated with PET measurement of  $\text{CMR}_{\text{O}_2}$  have also led to skepticism about the validity of the data that generated this controversial concept.

The resolution of this problem requires new studies, especially using techniques that avoid PET-specific errors. Mea-

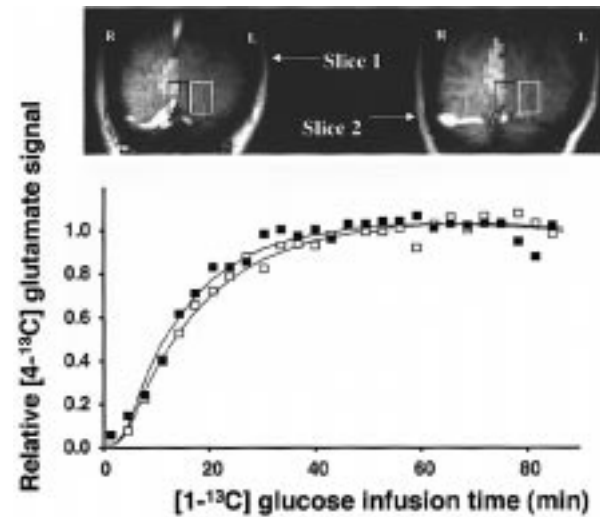


**Fig. 13.** Spectroscopic measurement of glutamate synthesis and oxygen consumption rate in the human brain using hemifield visual stimulation that selectively activates one hemisphere in the visual cortex. Spectroscopy data are acquired *simultaneously* from two 12 ml voxels. FMRI studies conducted together with the spectroscopy measurements delineate the activated region. This information is then used to position the voxels so that one is located in the activated region of the activated hemisphere, and the other in the corresponding nonactivated region in the other hemisphere. The image in gray scale is a coronal slice showing brain anatomy; the activated region appears in one hemisphere only. The boxes define the location of the voxels from which spectroscopic data were obtained. Time courses of glutamate labeling are shown for the control and activated regions in the brain [61].

surements in a single subject within a single experiment are also crucial in order to avoid large variances generated by intersubject averaging. This was recently accomplished in the human brain using isotopic turnover rate of glutamate from infused  $\{1-^{13}\text{C}\}$  glucose using indirect detection through coupled protons (Fig. 13). Glutamate labeling kinetics was followed for “activated” and resting states simultaneously in the same individual during hemifield visual stimulation by acquiring data in two distinct small volumes that span the

primary visual cortex [61], [77]. Hemifield visual stimulation selectively activates the primary visual cortex of the contralateral hemisphere, and thus approximately half the primary visual cortex volume that normally would be engaged during full field stimulation. Spectra can be acquired from two volumes positioned so that only one of the two covers the “activated” region within one hemisphere while the other covers the analogous but nonactivated region within the other hemisphere. Fig. 13 demonstrates an image showing the activation in one hemisphere, the location of the spectroscopic voxels and the time courses of glutamate labeling from the activated and control voxels. These data put an upper limit on the increase in  $CMR_{O_2}$  of 30% as opposed larger increases in CBF, supporting the concept that  $CMR_{O_2}$  is not stoichiometrically coupled increases in CBF and  $CMR_{glu}$ .

## REFERENCES

- [1] I. I. Rabi, J. R. Zacharias, S. Millman, and P. Kusch, “A new method of measuring nuclear magnetic moment,” *Phys. Rev.*, p. 318, 1938.
- [2] E. M. Purcell, H. C. Torrey, and R. V. Pound, “Resonance absorption by nuclear magnetic moments in a solid,” *Phys. Rev.*, vol. 69, pp. 37–38, 1945.
- [3] I. I. Rabi, S. Millman, and P. Kusch, “The molecular beam resonance method for measuring nuclear magnetic moments,” *Phys. Rev.*, vol. 55, pp. 526–535, 1939.
- [4] P. C. Lauterbur, “Image formation by induced local interaction: Examples employing nuclear magnetic resonance,” *Nature*, vol. 241, pp. 190–191, 1973.
- [5] S. Ogawa, T.-M. Lee, A. S. Nayak, and P. Glynn, “Oxygenation-sensitive contrast in magnetic resonance image of rodent brain at high magnetic fields,” *Magn. Reson. Med.*, vol. 14, pp. 68–78, 1990.
- [6] S. Ogawa and T. M. Lee, “Magnetic resonance imaging of blood vessels at high fields: *In vivo* and *in vitro* measurements and image simulation,” *Magn. Reson. Med.*, vol. 16, pp. 9–18, 1990.
- [7] S. Ogawa, T.-M. Lee, A. R. Kay, and D. W. Tank, “Brain magnetic resonance imaging with contrast dependence on blood oxygenation,” *Proc. Nat. Acad. Sci. USA*, vol. 87, pp. 9868–9872, 1990.
- [8] K. K. Kwong, J. W. Belliveau, D. A. Chesler, I. E. Goldberg, R. M. Weisskoff, B. P. Poncelet, D. N. Kennedy, B. E. Hoppel, M. S. Cohen, and R. Turner *et al.*, “Dynamic magnetic resonance imaging of human brain activity during primary sensory stimulation,” *Proc. Nat. Acad. Sci. USA*, vol. 89, no. 12, pp. 5675–5679, 1992.
- [9] P. A. Bandettini, E. C. Wong, R. S. Hinks, R. S. Tikofsky, and J. S. Hyde, “Time course *epi* of human brain function during task activation,” *Magn. Reson. Med.*, vol. 25, no. 2, pp. 390–397, 1992.
- [10] S. Ogawa, D. W. Tank, R. Menon, J. M. Ellermann, S. G. Kim, H. Merkle, and K. Ugurbil, “Intrinsic signal changes accompanying sensory stimulation: Functional brain mapping with magnetic resonance imaging,” *Proc. Nat. Acad. Sci. USA*, vol. 89, no. 13, pp. 5951–5955, 1992.
- [11] P. T. Fox and M. E. Raichle, “Focal physiological uncoupling of cerebral blood flow and oxidative metabolism during somatosensory stimulation in human subjects,” *Proc. Nat. Acad. Sci. USA*, vol. 83, no. 3, pp. 1140–1144, 1986.
- [12] P. T. Fox, M. E. Raichle, M. A. Mintun, and C. Dence, “Nonoxidative glucose consumption during focal physiologic neural activity,” *Science*, vol. 241, no. 4864, pp. 462–464, 1988.
- [13] M. E. Raichle, “Circulatory and metabolic correlates of brain function in normal humans,” in *Handbook of Physiology—The Nervous System*, 1987, pp. 643–674.
- [14] D.-S. Kim, T. Duong, and S.-G. Kim, “High-resolution mapping of iso-orientation columns by fMRI,” *Nature Neurosci.*, vol. 3, no. 2000, pp. 164–169.
- [15] Q. D. Duong, D.-S. Kim, K. Ugurbil, and K. S.-G., “Spatio-temporal dynamics of bold fMRI signals: Toward mapping submillimeter cortical columns using the early negative response,” *Magn. Reson. Med.*, vol. 44, no. 2, pp. 231–242, 2000.
- [16] S. LeVay and S. B. Nelson, *Vision and Visual Dysfunction: Macmillan and Houndsmill*, 1991, pp. 266–315.
- [17] D. H. Hubel and T. N. Wiesel, “Receptive field, binocular interactions and functional architecture in the cat’s visual cortex,” *J. Physiol. Lond.*, vol. 160, pp. 106–154, 1962.
- [18] S. LeVay, M. P. Stryker, and C. J. Shatz, “Ocular dominance columns and their development in layer IV of the cat’s visual cortex: A quantitative study,” *J. Comp. Neurol.*, vol. 179, no. 1, pp. 223–244, 1978.
- [19] T. Bonhoeffer and A. Grinvald, “Iso-orientation domains in cat visual cortex are arranged in pinwheel-like patterns,” *Nature*, vol. 353, no. 6343, pp. 429–431, 1991.
- [20] D. S. Kim and T. Bonhoeffer, “Reverse occlusion leads to a precise restoration of orientation preference maps in visual cortex,” *Nature*, vol. 370, no. 6488, pp. 370–372, 1994.
- [21] P. E. Maldonado, I. Godecke, C. M. Gray, and T. Bonhoeffer, “Orientation selectivity in pinwheel centers in cat striate cortex,” *Science*, vol. 276, no. 5318, pp. 1551–1555, 1997.
- [22] A. Shmuel and A. Grinvald, “Functional organization for direction of motion and its relationship to orientation maps in cat area 18,” *J. Neurosci.*, vol. 16, no. 21, pp. 6945–6964, 1996.
- [23] M. C. Crair, D. C. Gillespie, and M. P. Stryker, “The role of visual experience in the development of columns in cat visual cortex,” *Science*, vol. 279, no. 5350, pp. 566–570, 1998.
- [24] N. V. Swindale, J. A. Matsubara, and M. S. Cynader, “Surface organization of orientation and direction selectivity in cat area 18,” *J. Neurosci.*, vol. 7, no. 5, pp. 1414–1427, 1987.
- [25] T. Ernst and J. Hennig, “Observation of a fast response in functional MR,” *Magn. Reson. Med.*, vol. 32, pp. 146–149, 1994.
- [26] J. Hennig, C. Janz, O. Speck, and T. Ernst, “Examination of the mechanism of the fast response in functional MR,” in *3rd Scientific Meeting Soc. Magnetic Resonance in Medicine*, Nice, France, 1995.
- [27] X. Hu, T. H. Le, and K. Ugurbil, “Evaluation of the early response in fMRI using short stimulus duration,” *Magn. Reson. Med.*, vol. 37, pp. 877–884, 1997.
- [28] R. S. Menon, S. Ogawa, X. Hu, J. P. Strupp, P. Anderson, and K. Ugurbil, “Bold based functional MRI at 4 Tesla includes a capillary bed contribution: Echo-planar imaging correlates with previous optical imaging using intrinsic signals,” *Magn. Reson. Med.*, vol. 33, no. 3, pp. 453–459, 1995.
- [29] D. B. Twieg, G. G. Moore, and Y. T. Zhang, “Estimating fast response onset time,” in *Int. Soc. Magnetic Resonance in Medicine. 5th Scientific Meeting*, Vancouver, BC, Canada, 1997.
- [30] A. Grinvald, H. Slovov, and I. Vanzetta, “Non-invasive visualization of cortical columns by fMRI,” *Nature Neurosci.*, vol. 3, pp. 105–107, 2000.
- [31] D. Malonek and A. Grinvald, “Interactions between electrical activity and cortical microcirculation revealed by imaging spectroscopy: Implication for functional brain mapping,” *Science*, vol. 272, pp. 551–554, 1996.
- [32] I. Vanzetta and A. Grinvald, “Increased cortical oxidative metabolism due to sensory stimulation: Implications for functional brain imaging,” *Science*, vol. 286, no. 5444, pp. 1555–1558, 1999.
- [33] S.-G. Kim, “Quantification of relative cerebral blood flow change by flow-sensitive alternating inversion recovery (fair) technique: Application to functional mapping,” *Magn. Reson. Med.*, vol. 34, pp. 293–301, 1995.
- [34] R. E. Edelman, B. Siewer, D. G. Darby, V. Thangaraj, A. C. Nobre, M. M. Mesulam, and S. Warach, “Quantitative mapping of cerebral blood flow and functional localization with echo-planar MR imaging and signal targeting with alternating radio frequency,” *Radiology*, vol. 192, pp. 513–520, 1994.
- [35] S.-G. Kim and N. V. Tsekos, “Perfusion imaging by a flow-sensitive alternating inversion recovery (fair) technique: Application to functional brain imaging,” *Magn. Reson. Med.*, vol. 37, no. 3, pp. 425–435, 1997.
- [36] S. G. Kim and K. Ugurbil, “Comparison of blood oxygenation and cerebral blood flow effects in fMRI; Estimation of relative oxygen consumption change,” *Magn. Reson. Med.*, vol. 38, no. 1, pp. 59–65, 1997.
- [37] E. C. Wong, R. B. Buxton, and L. R. Frank, “Quantitative imaging of perfusion using a single subtraction (Quiess and Quiess II),” *Magn. Reson. Med.*, vol. 39, no. 5, pp. 702–708, 1998.
- [38] D. A. Roberts, J. A. Detre, L. Bolinger, E. K. Insko, and J. S. Leigh, “Quantitative magnetic resonance imaging of human brain perfusion at 1.5 t using steady-state inversion of arterial water,” *Proc. Nat. Acad. Sci. USA*, vol. 91, pp. 33–37, 1994.

- [39] K. K. Kwong, D. A. Chesler, R. M. Weisskoff, K. M. Donahue, T. L. Davis, L. Ostergaard, T. A. Campbell, and B. R. Rosen, "MR perfusion studies with T1-weighted echo planar imaging," *Magn. Reson. Med.*, vol. 34, pp. 878–887, 1995.
- [40] J. A. Detre, W. Zhang, D. A. Roberts, A. C. Silva, D. S. Williams, D. J. Grandis, A. P. Koretsky, and J. S. Leigh, "Tissue specific perfusion imaging using arterial spin labeling," *NMR Biomed.*, vol. 7, no. 1–2, pp. 75–82, 1994.
- [41] J. A. Detre, J. S. Leigh, D. S. Williams, and A. P. Koretsky, "Perfusion imaging," *Magn. Reson. Med.*, vol. 23, pp. 37–45, 1992.
- [42] R. B. Buxton and L. R. Frank, "A model for the coupling between cerebral blood flow and oxygen metabolism during neural stimulation," *J. Cereb. Blood Flow Metab.*, vol. 17, no. 1, pp. 64–72, 1997.
- [43] N. V. Tsekos, F. Zhang, H. Merkle, M. Nagayama, C. Iadecola, and S. G. Kim, "Quantitative measurements of cerebral blood flow in rats using the fair technique: Correlation with previous iodoantipyrine autoradiographic studies," *Magn. Reson. Med.*, vol. 39, no. 4, pp. 564–573, 1998.
- [44] R. G. Pautler, A. C. Silva, and A. P. Koretsky, "In vivo neuronal tract tracing using manganese-enhanced magnetic resonance imaging," *Magn. Reson. Med.*, vol. 40, no. 5, pp. 740–748, 1998.
- [45] Y. J. Lin and A. P. Koretsky, "Manganese ion enhances T1-weighted MRI during brain activation: An approach to direct imaging of brain function," *Magn. Reson. Med.*, vol. 38, no. 3, pp. 378–388, 1997.
- [46] T. Duong *et al.*, *Int. Soc. Magnetic Resonance*, 2001.
- [47] K. R. Thulborn, J. C. Waterton, and P. M. Matthews. "Dependence of the transverse relaxation time of water protons in whole blood at high field," *Biochem. Biophys. Acta.*, vol. 714, pp. 265–272, 1992.
- [48] K. R. Thulborn, J. C. Waterton, P. M. Matthews, and G. K. Radda, "Oxygenation dependence of the transverse relaxation time of water protons in whole blood at high field," *Biochem. Biophys. Acta.*, vol. 714, pp. 265–270, 1982.
- [49] E. O. Stejskal and J. E. Tanner, "Spin diffusion measurements: Spin-echoes in the presence of a time dependent field gradient," *J. Chem. Phys.*, vol. 42, pp. 288–292, 1965.
- [50] A. W. Song, E. C. Wong, S. G. Tan, and J. S. Hyde, "Diffusion weighted fMRI at 1.5 T," *Magn. Reson. Med.*, vol. 35, no. 2, pp. 155–158, 1996.
- [51] J. L. Boxerman, P. A. Bandettini, K. K. Kwong, J. R. Baker, T. L. Davis, B. R. Rosen, and R. M. Weisskoff, "The intravascular contribution to fMRI signal change: Monte Carlo modeling and diffusion-weighted studies *in vivo*," *Magn. Reson. Med.*, vol. 34, no. 1, pp. 4–10, 1995.
- [52] R. M. Henkelman, J. J. Neil, and Q. S. Xiang, "A quantitative interpretation of Ivim measurements of vascular perfusion in the rat brain," *Magn. Reson. Med.*, vol. 32, no. 4, pp. 464–469, 1994.
- [53] G. A. Wright, B. S. Hu, and A. Macovski, "Estimating oxygen saturation of blood *in vivo* with MR imaging at 1.5 T," *J. Magn. Reson. Imag.*, vol. 1, no. 3, pp. 275–283, 1991.
- [54] S.-P. Lee, A. C. Silva, K. Ugurbil, and K. S.-G., "Diffusion weighted spin echo fMRI at 9.4 T: Microvascular/tissue contribution to bold signal changes," *Magn. Reson. Med.*, vol. 42, no. 5, pp. 919–928, 1999.
- [55] K. Ugurbil, S. Ogawa, S.-G. Kim, X. Hu, W. Chen, and X.-H. Zhu, "Imaging brain activity using nuclear spins," in *Magnetic Resonance and Brain Function*, B. Maraviglia, Ed. Amsterdam, The Netherlands: Societa Italiana di Fisica and IOS Press, 1999, pp. 261–301.
- [56] K. Ugurbil, X. Hu, W. Chen, X.-H. Zhu, S.-G. Kim, and A. Georgopoulos, "Functional mapping in the human brain using high magnetic fields," *Philos. Trans. R. Soc. Lond. B. Biol. Sci.*, vol. 354, no. 1387, pp. 1195–1213, 1999.
- [57] K. Ugurbil, W. Chen, X. Hu, S.-G. Kim, S. Ogawa, and X.-H. Zhu, "Functional MRI at high fields: Practice and utility," in *Methods in Biomedical Magnetic Resonance Imaging and Spectroscopy*, I. Yong, Ed. Chichester, U.K.: Wiley, 2000, pp. 603–623.
- [58] S. Lai, A. L. Hopkins, E. M. Haacke, D. Li, B. A. Wasserman, P. Buckley, L. Friedman, H. Meltzer, P. Hedera, and R. Friedland, "Identification of vascular structures as a major source of signal contrast in high resolution 2d and 3d functional activation imaging of the motor cortex at 1.5 t: Preliminary results," *Magn. Reson. Med.*, vol. 30, no. 3, pp. 387–392, 1993.
- [59] S. Ogawa, T. M. Lee, R. Stepnoski, W. Chen, X. H. Zhu, and K. Ugurbil, "An approach to probe some neural systems interaction by functional MRI at neural time scale down to milliseconds [in process citation]," *Proc. Nat. Acad. Sci. USA*, vol. 97, no. 20, pp. 11 026–11 031, 2000.
- [60] F. Hyder, J. R. Chase, K. L. Behar, G. F. Mason, M. Siddeek, D. L. Rothman, and R. G. Shulman, "Increased tricarboxylic acid cycle flux in rat brain during forepaw stimulation detected with 1h [13c] NMR," *Proc. Nat. Acad. Sci. USA*, vol. 93, no. 15, pp. 7612–7617, 1996.
- [61] W. Chen, R. Gruetter, X.-H. Zhu, B. Seaquist, and K. Ugurbil, "Study of oxygen utilization changes in human visual cortex during hemifield stimulation using 1h-{13c} MRS and fMRI," *Proc. Int. Soc. Magn. Reson. Med.*, vol. 8, p. 438, 2000.
- [62] F. Hyder, D. L. Rothman, G. F. Mason, A. Rangarajan, K. L. Behar, and R. G. Shulman, "Oxidative glucose metabolism in rat brain during single forepaw stimulation: A spatially localized 1h [13c] nuclear magnetic resonance study," *J. Cereb. Blood Flow Metab.*, vol. 17, no. 10, pp. 1040–1047, 1997.
- [63] R. Gruetter, E. J. Novotny, S. D. Boulware, G. F. Mason, D. L. Rothman, J. W. Prichard, and R. G. Schulman, "Localized 13c NMR spectroscopy of amino acid labeling from [1–13c] D-glucose in the human brain," *J. Neurochem.*, vol. 63, pp. 1377–1385, 1994.
- [64] N. R. Sibson, A. Dhankhar, G. F. Mason, K. L. Behar, D. L. Rothman, and R. G. Shulman, "In vivo 13c NMR measurements of cerebral glutamine synthesis as evidence for glutamate-glutamine cycling," *Proc. Nat. Acad. Sci. USA*, vol. 94, no. 6, pp. 2699–2704, 1997.
- [65] R. Gruetter, E. R. Seaquest, S. W. Kim, and K. Ugurbil, "Localized in vivo 13c NMR of glutamate metabolism in the human brain. Initial results at 4 Tesla," *Dev. Neurosci.*, vol. 20, no. 4–5, pp. 380–388, 1998.
- [66] J. Shen, K. F. Petersen, K. L. Behar, P. Brown, T. W. Nixon, G. F. Mason, O. A. Petroff, G. I. Shulman, R. G. Shulman, and D. L. Rothman, "Determination of the rate of the glutamate/glutamine cycle in the human brain by *in vivo* 13c NMR," *Proc. Nat. Acad. Sci. USA*, vol. 96, no. 14, pp. 8235–8240, 1999.
- [67] R. Gruetter, B. Seaquist, and K. Ugurbil, "A mathematical model of compartmentalized neurotransmitter metabolism in the human brain," *Amer. J. Physiol.*, 2001, to be published.
- [68] K. Ugurbil, T. R. Brown, J. A. den Hollander, P. Glynn, and R. G. Shulman, "High-resolution 13c nuclear magnetic resonance studies of glucose metabolism in *escherichia coli*," in *Proc. Nat. Acad. Sci. USA*, vol. 75, 1978, pp. 3742–3746.
- [69] R. Gruetter, "Automatic, localized *in vivo* adjustment of all first- and second-order shim coils," *Magn. Reson. Med.*, vol. 29, no. 6, pp. 804–811, 1993.
- [70] R. Gruetter, G. Adriany, H. Merkle, and P. M. Andersen, "Broadband decoupled, 1h-localized 13c MRS of the human brain at 4 tesla," *Magn. Reson. Med.*, vol. 36, no. 1, pp. 659–664, 1996.
- [71] G. Adriany and R. Gruetter, "A half volume coil for efficient proton decoupling in humans at 4 tesla," *J. Magn. Reson.*, vol. 125, pp. 178–184, 1997.
- [72] J. Pfeuffer, I. Tkac, I. Y. Choi, H. Merkle, K. Ugurbil, M. Garwood, and R. Gruetter, "Localized in vivo 1h NMR detection of neurotransmitter labeling in rat brain during infusion of [1-13c] D-glucose," *Magn. Reson. Med.*, vol. 41, no. 6, pp. 1077–1083, 1999.
- [73] D. E. Bergles, J. A. Dzubay, and C. E. Jahr, "Glutamate transporter currents in Bergmann Glial cells follow the time course of extrasynaptic glutamate," in *Proc. Nat. Acad. Sci. USA*, vol. 94, 1997, pp. 14 821–14 825.
- [74] D. E. Bergles, J. S. Diamond, and C. E. Jahr, "Clearance of glutamate inside the synapse and beyond," *Curr. Opin. Neurobiol.*, vol. 9, no. 3, pp. 293–298, 1999.
- [75] A. Martinez-Hernandez, K. P. Bell, and N.M. D., "Glutamine synthetase: Glial localization in brain," *Science*, vol. 195, pp. 1356–1358, 1976.
- [76] N. R. Sibson, A. Dhankhar, G. F. Mason, D. L. Rothman, K. L. Behar, and R. G. Shulman, "Stoichiometric coupling of brain glucose metabolism and glutamatergic neuronal activity," *Proc. Nat. Acad. Sci. USA*, vol. 95, no. 1, pp. 316–321, 1998.
- [77] W. Chen, X.-H. Zhu, R. Gruetter, and E. R. Seaquist, "Study of tricarboxylic acid cycle flux changes in human visual cortex during Hemifield visual stimulation using 1h-{13c} MRS and fMRI," *Magn. Reson. Med.*, 2001, to be published.
- [78] B. Siesjo, *Brain Energy Metabolism*. New York: Wiley, 1978, pp. 101–110.
- [79] T. Q. Duong, A. C. Silva, S. P. Lee, and S. G. Kim, "Functional MRI of calcium-dependent synaptic activity: Cross correlation with CBF and bold measurements [in process citation]," *Magn. Reson. Med.*, vol. 43, no. 3, pp. 383–392, 2000.

[80] D. S. Kim and T. Bonhoeffer, "Reverse occlusion leads to a precise restoration of orientation preference maps in visual cortex," *Nature*, vol. 372, no. 6502, p. 196, Nov. 10, 1994.

**Kamil Ugurbil**, photograph and biography not available at the time of publication.

**Dae-Shik Kim**, photograph and biography not available at the time of publication.

**Tim Duong**, photograph and biography not available at the time of publication.

**Xiaoping Hu** (Member, IEEE), photograph and biography not available at the time of publication.

**Seiji Ogawa**, photograph and biography not available at the time of publication.

**Rolf Gruetter**, photograph and biography not available at the time of publication.

**Wei Chen**, photograph and biography not available at the time of publication.

**Seong-Gi Kim**, photograph and biography not available at the time of publication.

**Xiao-Hung Zhu**, photograph and biography not available at the time of publication.

**Essa Yacoub**, photograph and biography not available at the time of publication.

**Pierre-Francois van de Moortele**, photograph and biography not available at the time of publication.

**Amir Shmuel**, photograph and biography not available at the time of publication.

**Josef Pfeuffer**, photograph and biography not available at the time of publication.

**Hellmut Merkle**, photograph and biography not available at the time of publication.

**Peter Andersen**, photograph and biography not available at the time of publication.

**Gregor Adriany**, photograph and biography not available at the time of publication.